
Article:
Amendola, A., Hernandez-Nava, E., Goodall, R. et al. (2015) On the additive manufacturing, post-tensioning and testing of bi-material tensegrity structures. Composite Structures, 131. 66 - 71. ISSN: 0263-8223

https://doi.org/10.1016/j.compstruct.2015.04.038

On the additive manufacturing and testing of tensegrity structures

A. Amendola

Department of Civil Engineering, University of Salerno,84084 Fisciano(SA), Italy

E. Hernández-Nava, R. Goodall, I. Todd

Department of Materials Science and Engineering, University of Sheffield, Mappin Street, Sheffield, S1 3JD, UK

R.E. Skelton

University of California San Diego, MAE/Aero, 9500 Gilman Dr., La Jolla, CA 92093, USA

F. Fraternali

Department of Civil Engineering, University of Salerno,84084 Fisciano(SA), Italy

Abstract

An investigation on the additive manufacturing and the experimental testing of 3D models of tensegrity prisms and columns is presented. An electron beam melting facility (Arcam EBM S12) is employed to 3D print structures composed of tensegrity prisms endowed with rigid bases and temporary supports, which are made out of the titanium alloy Ti6Al4V. The temporary supports are removed after the additive manufacturing phase, when Spectra cross-strings are added to the 3D printed models, and a suitable state of internal prestress is applied to the structure. The experimental part of the study shows that the examined structures feature sitffening-type elastic response under large or moderately large axial strains induced by compressive loading. Such a geometrically nonlinear behavior confirms previous theoretical results available in the literature, and paves the way to the use of tensegrity prisms and columns as innovative mechanical metamaterials and smart devices.

Keywords: Tensegrity Structures, Additive Manufacturing, Electron Beam Melting, Post-tensioning, Geometrically Nonlinear Behavior, Elastic Stiffening

1. Introduction

One of the most common techniques nowadays employed for the fabrication and the rapid prototyping of innovative periodic structures and lattice materials is additive manufacturing (AM). Several fabrication methods have been proposed in this field, with

Email addresses: adaamendola1@unisa.it (A. Amendola), mtq10eh@sheffield.ac.uk (E. Hernández-Nava, R. Goodall, I. Todd), bobskelton@ucsd.edu (R.E. Skelton), f.fraternali@unisa.it (F. Fraternali)

resolution ranging from the centimetre- to the nanometre-scale. It is worth mentioning polyjet 3d printing technologies; Electron Beam Melting (EBM); x-ray lithography; deep UltraViolet lithography; soft lithography; two-photon polymerization; atomic layer deposition; and projection micro-stereolitography, among other available methods (refer to (Bückmann, 2014), (Maldovan, 2013), (Meza et al., 2014), (Grunsven et al., 2014), (Zheng et al., 2012), and references therein). The processing of detailed components through the consecutive addition of small quantities of material, usually in thinner layer than 100 μm, makes AM capable of producing highly complex structures at different scales. EBM is a popular AM technique used to fabricate metallic structures. Its name is own to the technique's deposition, in which, it makes use of a beam of electrons to fully melt powder particles of a conductive material. This melting operation is performed in a selectively way through a surface file, commonly STL. The use of EBM has been successfully demonstrated in several studies of structured materials as; lattices with graded porosity (Grunsven et al., 2014), metallic foams (Hernández-Nava et al., 2015), optimized topologies Smith et al. (2014) and structures with negative Poisson's ratio (Cormier et al., 2012) to name a few.

Tensegrity structures are axially loaded prestressable structures. Motivated by nature, where tensegrity concepts recurrently appear (Skelton and de Oliveira, 2010c), engineers have only recently developed efficient analytical methods to exploit tensegrity concepts in engineering design. Traditional construction of tensegrity structures through manually assembling of different components can represent a challenging task. Potentially resulting in a series of mitigated results because of structural and connecting issues; eccentricities at the joints, unwanted movements and friction (refer, e.g., to (Amendola et al., 2012) and references therein). Hence in order to systematically study complex tensegrity systems, the development of fabrication techniques based on AM would be of great help.

The present work investigates on the quasi-static response under axial compressive loading of bi-material models of tensegrity structure partially produced through EBM. The paper begins by describing the Computer Aided Design (CAD) of the structures to be 3D printed, which include one or more building blocks (tensegrity prisms) formed by three titanium alloy (Ti6Al4V) bars; two Ti6Al4V plates (bases), and three Spectra fibers connecting the base plates (Sect. 2). Sect. 3 describes the EBM process used for the AM manufacturing of temporary models without the Spectra fibers, while Sect. 4 illustrates the placement and the post-tensioning of such elements within the final structures. The experimental part of the study present quasi-static compression tests that investigate on the response of the examined structures under compressive axial loading. The given results validate the theoretical predictions presented in (Amendola et al., 2012; Fraternali et al., 2014a), highlighting the geometrically non-linear nature of the axial force vs. axial displacement response of such structures (Sect. 5). We end in Sect. 6, by drawing the main conclusions of the present study and future research lines.

2. Geometric models of tensegrity prisms and columns

We focus in the present Section on the computer aided design of provisional models of structures showing tensegrity prisms endowed with rigid bases as building blocks (Amendola et al., 2012). Each prism is composed of three struts, two rigid bases (a top-base, and a bottom-base), and three cross-cables.

Figs. 1, 2 show a computer models of metallic structures formed by the struts and the terminal bases of the building blocks, plus some sacrificial supports connecting the bases of the building blocks (vertical elements in Figs. 1, 2). The connections between the bars and the bases are realized through hemispherical (terminal blocks) or spherical (internal blocks) joints (cf. Figs. 1, 2). Such provisional structures will be additively manufactured in a titanium alloy (Ti6Al4V) through the EBM facility Arcam S12 (cf. Sect. 3). Next, the 3D printed structures will be finished with the addition of tensioned Spectra strings connecting the struts and the terminal bases of the building blocks. Once the insertion of the Spectra strings will be completed, and a suitable prestress will be applied to the structure, the sacrificial supports will be removed (*post-tensioning approach*, cf. Sect.4).

Let's show in detail how we design the building blocks of the structures under investigation. To ensure zero bending moments, the extremities of the bars composing such units should have almost zero diameter at the nodes. Unfortunately, it is impossible to additively manufacture elements with nearly zero diameter, due to the limited precision tolerance of the available printing machine. Indeed, the ARCAM A2X EBM facility allows to smoothly manufacture features with size not smaller than 0.5 mm (Hernández-Nava et al., 2015). Such a limitation also affects the manufacturing of the tensile elements (cables or strings) of the building blocks, due to the small diameter that is needed for such elements. As we already explained, our fabrication strategy makes use of 3D printed temporary models in which the strings are replaced by sacrificial with diameter $d^* = 0.5$ mm. The latter are removed in a second phase, when Spectra strings are manually inserted into the building blocks, with the aim of 'sewing' the 3D printed models (Sect.4). To this end, the models to be 3D printed show holes passing through the joints, which will host the Spectra strings in the post-tensioning phase. We design the compressive elements (bars or struts) of the temporary models with a bi-conic shape obtained by joining two truncated cones. The latter feature decreasing radii towards the extremities (Fig. 1), so as to minimize the bending rigidity of the nodes. Let d denote the minimum diameter of the struts (at the extremities), and let D denote the maximum diameter of such elements (at the mid-span). Following Kadic et al. (2012) we make use of the following tapering ratio: $\beta = D/d = 6$.

Overall, each building block to be 3D printed is composed of three truncated bi-cones (bars), three tacrificial supports, two triangular plates of thickness t (bases), and six semi-spherical or spherical joints with radius r (Fig. 1). Table 1 shows the geometric properties of such elements, making use of the symbols s_N, b_N and h_N to respectively denote the length of the edges of the base plates; the length of the struts; and the height of the prism (measured from the centre to centre of the bases), in correspondence with the unstressed (or natural) configuration of the structure. Fig. 2 shows temporary models of tensegrity columns obtained by superimposing different numbers of building blocks. Each block can be either 'right-handed' or 'left-handed', depending whether the upper base is clockwise or counter-clockwise twisted with respect to the lower base, respectively. The examined columns can stack blocks with the same orientation (Fig. 2x-y), or blocks with different orientations (Fig. 2z-w).

Figure 1: Graphical model of a building block composed of three sacrificial supports (yellow), six semi-spherical joints (orange), three struts (blue) and two terminal plates (gray).

t (mm)	r (mm)	s_N (mm)	b_N (mm)	D(mm)	d (mm)	d^* (mm)	h_N (mm)
1.0	1.5	22.0	30.8	3.0	0.5	0.5	20.7

Table 1: Geometrical properties of the building blocks of the examined models

3. Additive manufacturing of physical models

The present section focuses on the EBM technique employed to process the CAD models illustrated in the previous section. We begin by describing the geometrical and chemical characteristics of the employed Ti6Al4V alloy Next, we briefly describe the employed manuacturing process. We end by presenting an experimental study on the of the influence of the EBM angle deposition on the mechanical properties of the melted Ti-6Al-4V alloy.

3.1. Raw materials

The manufacturing process examined in the present work starts with the insertion of a Ti4Al6V prealloyed powder into the build platform of the printing machine (Arcam EBM S12). Such a powder is provided by the manufacturer and is made of spherical particles with $45 - 100$ μ m diameter. The raw material obeys the standards of the American Society of Testing and Materials (ASTM GRade 5, 6al-4V) (ASTM F1108, 2014) It must be considered, however, that the continuous material reuse, which is a common practice in the EBM manufacturing, might slightly change the chemical composition of the Ti6Al4V powder. Tab. 3.1 provides the chemical composition experimentally determined for the powder employed in the previous study.

Table 2: Chemical composition of the Ti-6Al-4V prealloyed powder in wt%.

Ti	Al	V	Fe	C	N	O
88.28	6.88	4.27	0.18	0.007	0.026	0.33

3.2. Manufacturing process

EBM works in vacuum conditions at 1.9×10^{-3} mbar, by heating the base of the build area up to the temperature of 720∘C. Layers of Ti-6Al-4V powder are progressively

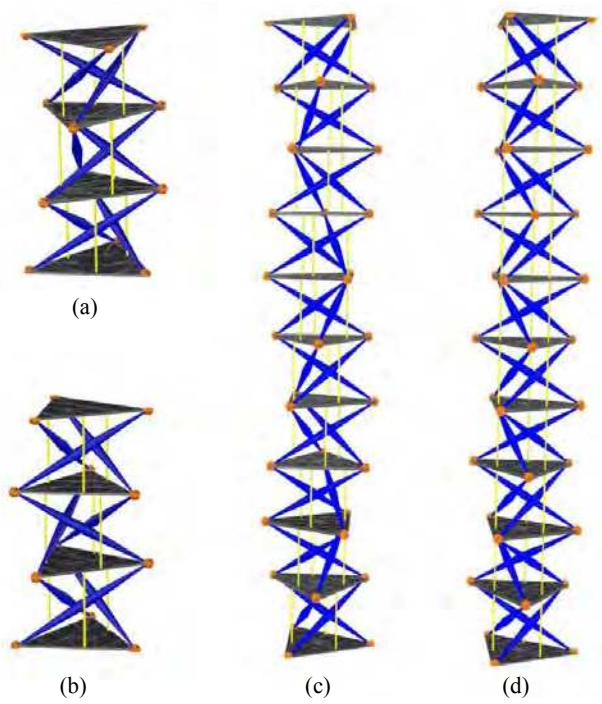

Figure 2: Collection of tensegrity columns to be 3D printed using different numbers of prisms and different orientations: (a) column with three left-handed prisms, (b) column with three left-right handed prisms, (c) column with ten left-handed prisms, (d) column with ten left-right handed prisms.

deposited, heated and melted, according to a sliced version of the CAD model to be manufactured, which is prepared by an internal preprocessor of the Arcam EBM S12. Layer heating (using a defocused beam) is employed to reduce the energy needed for the melting phase. The EBM working parameters are varied for the bars, joints and plates, with the of ensuring uniform material density throughout the model, as much as possible (cf. Tab, 3). The voltage is kept constant at 60kV. Once manufactured, all remnants of unmelted powder are removed using compressed air.

Table 3: Beam parameters employed for the manufacturing of the model parts.

	Beam current (mA)	Beam speed (mm/s)	Focus Offset
Preheat	30	14600	50
Plates	17	500	19
Spheres	1.7	200	0
Bars	1.7	200	0

3.3. Parent material properties

We printed twelve tensegrity prisms with two different building orientations for material characterization purposes. The min goal of such a study was to detect the influence of the EBM angle deposition on the mechanical properties of the melted Ti-6Al-4V alloy.

We built six samples along the vertical direction (V specimens: prism bases parallel to the building plate), and six other samples along the horizontal direction (H specimens: prism bases perpendicular to the building plate). Parts of such specimens, manually cut through tongs, were subject to tensile tests according to the ASTM standard E8-13a (ASTM E8 - 13a, 2014). The data obtained from tensile tests include the 0.2 % Yield strength (YS), ultimate tensile strength (UTS), and Young's modulus (YM), see Table 4. The yield strength of V- and H-specimens was found slightly different (V-specimens more resistant than H-specimens, cf. Table 4), mainly due to changes in material porosity with the deposition angle (Murr et al., 2010). It is worth mentioning that the replicability of material properties in the AM of lattice materials is subject of debate. This as the fraction of defects, such as internal porosity and surface roughness, dramatically affect the material strength, especially in the case of small features, such as, e.g., the nodal junctions (Hernández-Nava et al., 2015). The results presented in Table 4 led us to prefer the vertical deposition technique for the manufacturing of the final specimens (Figs. 3, 4 and 5).

Table 4: Bulk material properties based on tensile tests for two build orientations.

Build orientation	0.2 % Y.S.	UTS	Young's modulus
	(MPa)	(MPa)	(GPa)
Horizontal	881± 8.4	1040±6.7	110±2.1
Vertical	923±10.7	1042±9.2	116±2.8

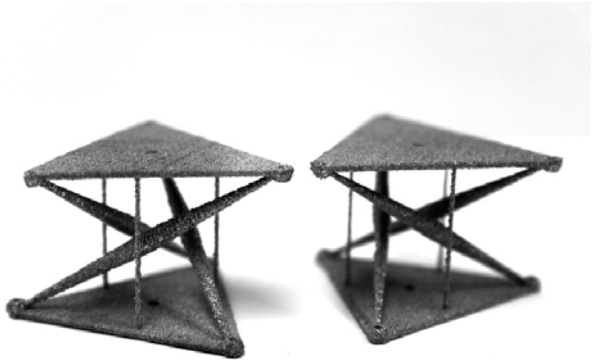

Figure 3: EBM-printed left-handed (left) and rigth-handed (right) tensegrity prisms.

4. Post-tensioning of 3D printed specimens

As anticipated, we 'sewed' the 3D printed structures by slipping Spectra® fibers with 0.1 mm diameter through the holes crossing the joints. We used Spectra fibers commercialized by Shimano American Corporation (Irvine, CA, USA), with declared maximum strength of 5 Kg. Hereafter, we assume that such string elements have Young modulus E_s=5.48GPa, based on the results of the experimental study presented in (Amendola et al., 2012). Since the cross-section area of the strings is $A_s = \pi\ 0.1^2/4 = 0.0078$ mm^2,

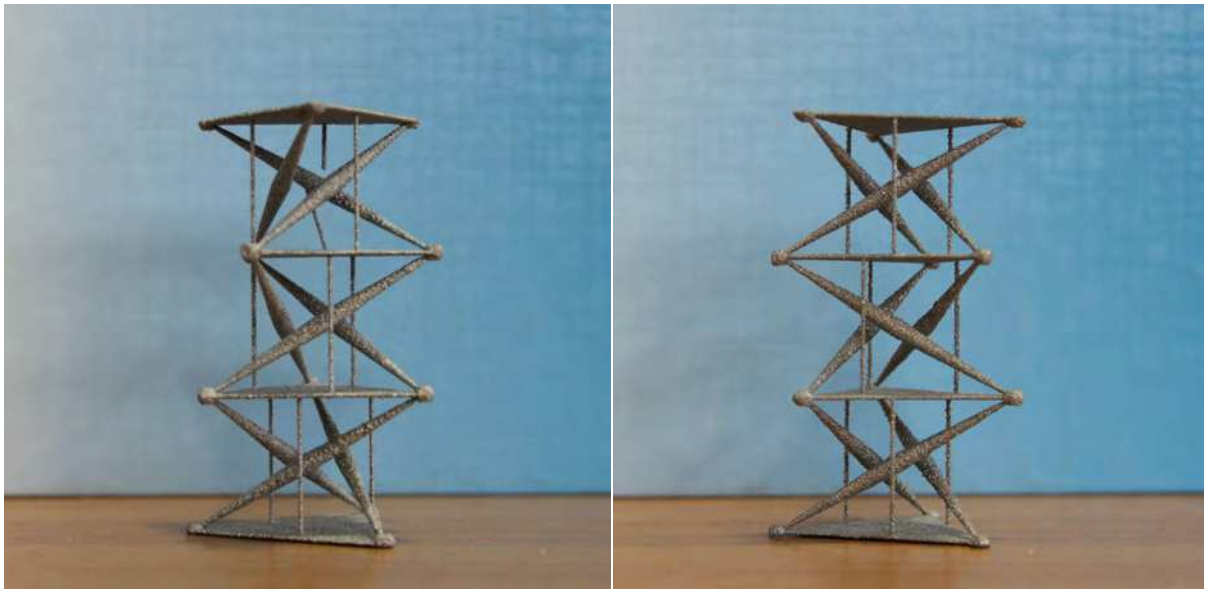

Figure 4: EBM-printed columns with three left-handed prisms (left), and three left-rigth handed prisms (rigth).

their axial stiffness is computed as: $E_s A_s = 0.043$ kN. After slipping the Spectra strings through the holes crossing the joints, we fixed them in correspondence with the top-base of the structure through slipknots (Fig. 6). Next, we removed the sacrificial supports of the 3D printed structure (cf. Figs. 3, 4 and 5), and we tensioned the strings by fixing them to the bottom-base. A level was placed on the top-base of the structure during the post-tensioning phase, in order to ensure that such a base was horizontal, and the strings approximatively carried equal tensile forces. We applied the post-tension approach to manufacture single prisms, either left-handed (L-prisms, Fig. 6-left) or right-handed (R-prisms, Fig. 6-right); columns showing three left-handed prisms (3LLL-columns, Fig. 7-left); and columns showing two terminal left-handed prisms and one central right-handed prism (3LRL-columns, Fig. 7-right). We plan to apply the post-tensioning approach to ten-prism columns (Fig. 5) in future work.

5. Quasi-static compression tests

We investigated on the experimental response of the structures illustrated in the previous section under quasi-static compression loading, on employing a strain rate of $1{\cdot}10^3\ s^1$. The testing apparatus consisted of a Zwick/Roell Z050 testing machine equipped with 20 kN load cell (Fig.8). To minimize the frictional effects between the terminal bases of the prisms and the testing machine plates, we carefully lubricated all such surfaces, before initiating the compression tests. We lubricated the joints of the tested structures as well, in order to reduce the friction between the strings and the rough internal surface of the joints.

Fig. 9 shows the results of compression tests on different L-prisms and R-prisms, which differ from each other for the value of the applied prestress. The effective cross-string prestrain p of such specimens was in-situ measured through the identification procedure illustrated in Sect. 3.3 of Amendola et al. (2012). The axial force F vs. axial-displacement

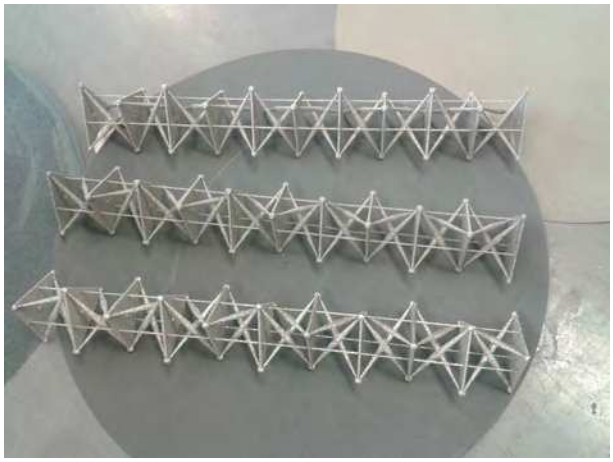

Figure 5: EBM-printed columns with ten building blocks, obtained by alternating left-handed and rigth-handed prisms.

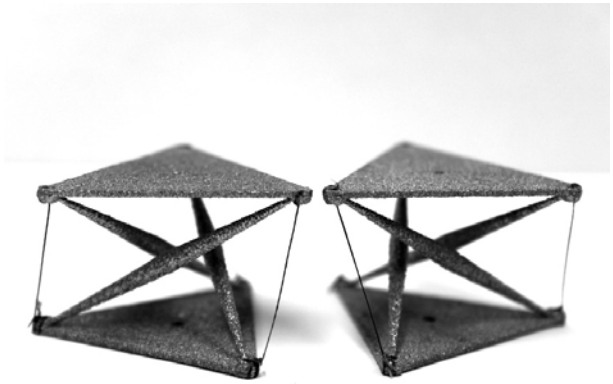

Figure 6: L-prims (left) and R-prism (right) prisms obtained by 'sewing' the EBM-printed models with Spectra strings.

δ plots in Fig. 9 highlight a marked stiffening behavior of the single-prism structures (tangent stiffness increasing with δ), up to the specimen failure, which confirms the theoretical predictions presented in Fraternali et al. (2014a). The specimen collapse was due to the detachment of one or more bars from the joints. It is worth mentioning that we didn't observe plastic yielding of the strings or buckling of the bars up to the specimen failure.

The force F vs. displacement δ curves of 3LLL and 3LRL specimens are shown in Fig. 10. We observe that the initial branches of the $F - \delta$ curves exhibited by such specimens are practically coincident, for $\delta \leq 2.50$ mm. As δ gets larger than such a threshold, we instead observe that $F - \delta$ curves of the 3LLL specimens get visibly stiffer than those exhibited by the 3LRL specimens. We also observe that the $F - \delta$ curves of the 3LLL specimens exhibit marked oscillations in the large displacement regime. This is explained by damage phenomena due to the marked rubbing of the cross-strings against the walls of the joint holes,l in such a regime. The collapse of the 3LLL specimens was

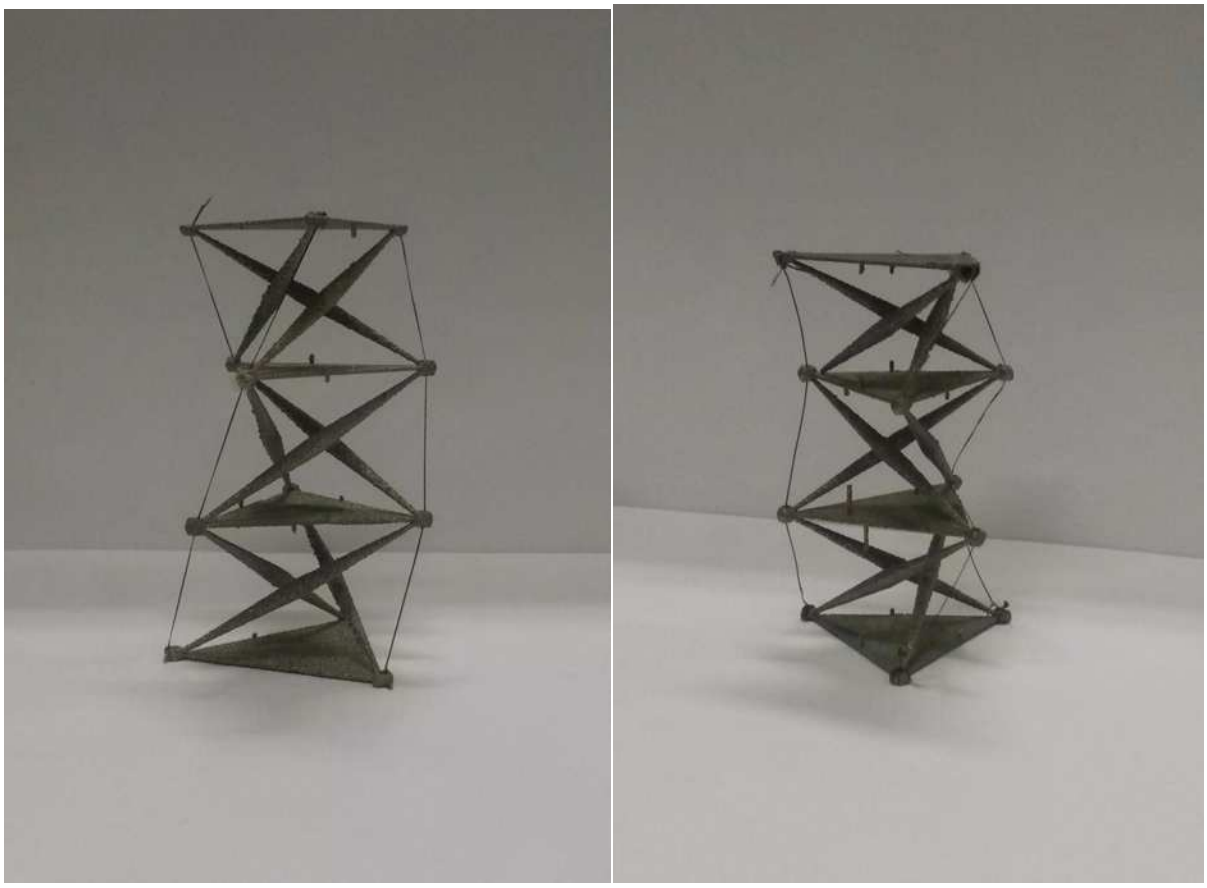

Figure 7: 3LLL (left) and 3LRL (right) columns obtained by 'sewing' the EBM-printed models with Spectra strings.

due to the detachment of the bars of the top-most prism from the upper joints, while that of the 3LRL specimens was due to the simultaneous detachment of the bars of the central prisms from upper and lower joints. It is worth remarking that the rupture of the 3LRL specimens occurred in correspondence with smaller axial displacements δ, as compared to that exhibited by the 3LLL specimens (Fig. 10). The anticipated failure of 3LRL specimens can be explained by the opposite twisting of the terminal prisms in such structures, which produces marked stress concentration at the interfaces between the terminal units and the central prism. Differently, in the 3LLL specimens, all the prisms twist counter clockwise, which produces limited stress concentration at the nodes, and allows the structure to sustain large axial displacements before failure. Overall, we may conclude that the response of the 3LRL specimens is affected by opposite-twisting effects of the terminal units, especially under large or moderatley large axial displacements, while that of the 3LLL specimens replicates the response of a single prism over a larger window of axial displacements (compare Figs. 9 and 10). In both cases, we observe a geometrically nonlinear response of the structure (more pronounced in the 3LRL specimens), which paves the way to the use of such structures as nonlinear mechanical metamaterials.

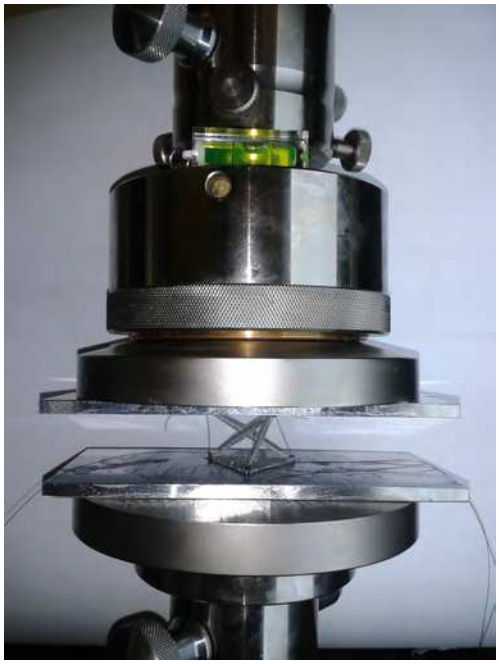

Figure 8: Experimental set-up for the compression testing of post-tensioned structures.

6. Concluding remarks

We have investigated on the fabrication of physical models of tensegrity structures, by combining the additive manufacturing of metallic models, via EBM, with the manual insertion of tensioned Spectra strings in 3D printed structures. Such a 'post-tensioning' approach has been applied to the construction of columns composed of different numbers of tensegrity prisms, which may feature either equal or opposite orientation (Skelton and de Oliveira, 2010c). In all the examined structures, the building blocks consist of tensegrity prisms endowed with rigid bases. Compression tests have been performed on single prisms and columns composed of three prisms, with the aim of characterizing the nature of the mechanical response of such structures under large or moderately large axial displacements. We have observed a markedly nonlinear response of the examined structures, and elastic hardening effects under large axial displacements. Such results confirms the outcomes of previous theoretical and experimental results available in the literature on the mechanical response of tensegrity prisms and columns endowed with rigid bases (Oppenheim and Williams, 2000; Fraternali et al., 2012; Amendola et al., 2012; Fraternali et al., 2014a,b).

Recent studies have shown that elastically hardening mechanical metamaterials support compressive solitary waves and the unusual reflection of waves on material interfaces (Nesterenko, 2001; Fraternali et al., 2012, 2014b). Solitary wave dynamics has been proven to be useful for the construction of a variety of novel acoustic devices. These include: acoustic band gap materials; shock protector devices; acoustic lenses; and energy trapping containers, to name some examples (refer, e.g., to Theocharis et al. (2013) and references therein). The present study represents a first step towards the additive manufacturing and testing of nonlinear tensegrity metatamerials to be employed for real-life

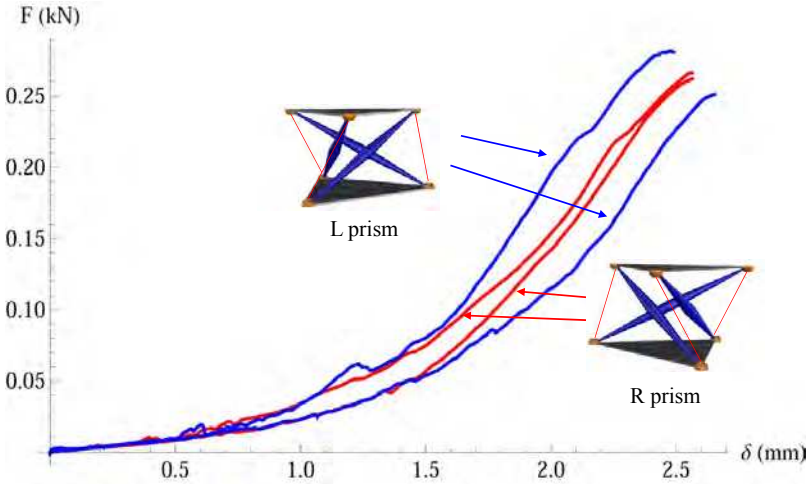

Figure 9: Axial force F vs. axial-displacement δ curves of single-prism structures under axial compression loads.

engineering devices. We address to future work the formulation and implementation of innovative, multimaterial deposition techniques that are able to apply internal prestress in AM-fabricated tensegrity structures. We plan to fabricate macro- and small-scale models of such structures using materials with different coefficients of thermal expansion for struts and cables. In addition, we plan to manufacture micro-scale tensegrity models through projection micro-stereolitography (Zheng et al., 2012), employing swelling materials for the tensile members (Lee et al., 2012). Once dried, such members will contract, creating internal prestress. Engineering applications of the above metamaterials will deal with novel, tunable focus acoustic lenses, and innovative devices for monitoring structural health and damage detection in materials and structures (Fraternali et al., 2012; Donahue et al., 2014; Ni, 2011).

Acknowledgements

Support for this work was received from the Italian Ministry of Foreign Affairs, Grant No. 00173/2014, Italy–USA Scientific and Technological Cooperation 2014–2015 ('*Lavoro realizzato con il contributo del Ministero degli Affari Esteri, Direzione Generale per la Promozione del Sistema Paese*').

References

ASTM F1108-14. Standard Specification for Titanium - 6Aluminum - 4Vanadium Alloy Castings for Surgical Implants, UNS R56406 *(2014)*, DOI: 10.1520/F1108-14.

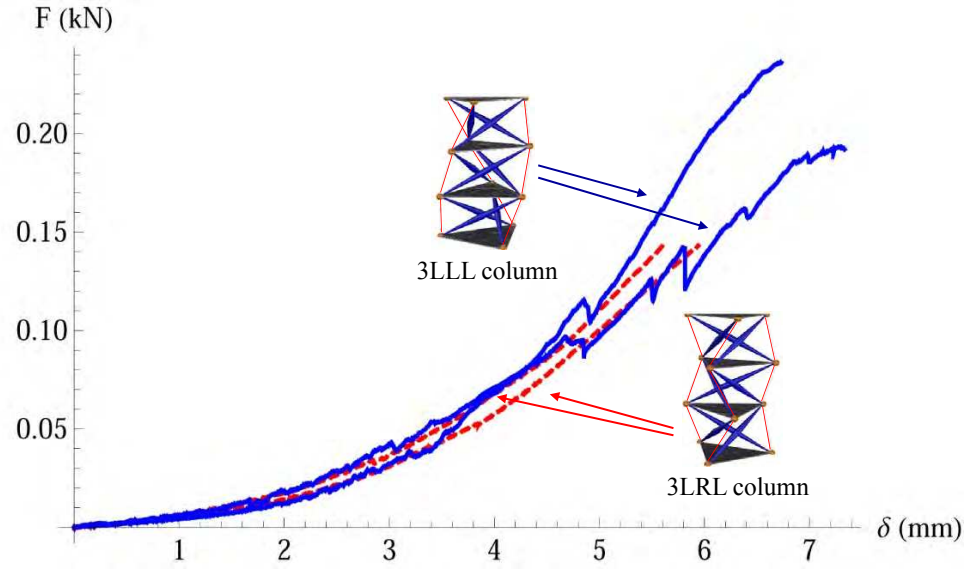

Figure 10: Experimental results of 3LLL column and 3LRL column under axial compression loads.

ASTM F1472 - 08e1. Standard Specification for Wrought Titanium-6Aluminum-4Vanadium Alloy for Surgical Implant Applications, UNS R56400 *(2008)*, DOI: 10.1520/F1472-08E01.

ASTM E8 - 13a. Standard Test Methods for Tension Testing of Metallic Materials, DOI 10.1520/E0008 E0008M.

Bel Hadj Ali, N., Rhode-Barbarigos, L., Pascual Albi, A. A., Smith, I. F. C., 2010. Design optimization and dynamic analysis of a tensegrity-based footbridge. Eng. Struct., 32(11),3650–3659.

Amendola, A., Fraternali, F., Carpentieri, G., de Oliveira, Skelton, R.E., 2014. Experimental investigation of the softening-stiffening response of tensegrity prisms under compressive loading. Compos. Struct., 117, 234-243.

Amendola, A., Nava, E.H., Goodall, R., Skelton, R.E., Fraternali, F., 2015. On the mechanical behavior of tensegrity columns manufactured through electron beam melting. Compos. Struct., in press.

Brunet, T., Leng, J., Mondain-Monva, O., 2013. Soft acoustic metamaterials. Science 342, 323–324.

Bückmann,T., Thiel, M., Kadic, M., Schittny, R., Wegener, M., 2014. An elastomechanical unfeelability cloak made of pentamode metamaterials. Nature Communications 5, 4130.

Yang, L., Harrysson, O., West, H., Cormier, D., Compressive properties of Ti6Al4V auxetic mesh structures made by electron beam melting. Acta Materialia, 60 (2012) 3370-3379.

Kadic, M., Bückmann, D., Stenger N., Thiel, M. and Wegner, M., 2012. On the practicability of pentamode mechanical metamaterials. Appl. Phys. Lett. 100, 191901.

Carpentieri, G., Skelton, R.E., Fraternali, F., (2014). Parametric design of minimal mass tensegrity bridges under yielding and buckling constraints. *In press, 2014. Eprint: arXiv:1411.7966 [cond-mat.mtrl-sci]. DOI: 10.13140/2.1.3224.2248.*

Daraio, C., Ngo, D., Nesterenko, V.F. and Fraternali, F., (2010). Highly nonlinear pulse splitting and recombination in a two-dimensional granular network. *Phys. Rev. E.*, 82:036603.

Donahue, C., Anzel, P., Bonanomi, L., Keller, T.; Daraio, C., (2014). Experimental realization of a nonlinear acoustic lens with a tunable focus. Appl. Phys. Lett., 104, 014103.

Fraternali, F., Porter, M., and Daraio, C., 2010. Optimal design of composite granular protectors. Mech. Adv. Mat. Struct. 17, 1–19.

Fraternali, F., Senatore, L. and Daraio, C., 2012. Solitary waves on tensegrity lattices. J.Mech. Phys. Solids 60, 1137–1144.

Fraternali, F., Carpentieri, G., Amendola, A. On the mechanical modeling of the extreme softening/stiffening response of axially loaded tensegrity prisms. J.Mech. Phys. Solids, In press (E-print, arXiv:1406.1913 [cond-mat.mtrl-sci], 2014).

Fraternali, F., Carpentieri, G., Amendola, A., Skelton, R.E., Nesterenko, V. F., 2014. Multiscale tunability of solitary wave dynamics in tensegrity metamaterials. Appl. Phys. Lett. 105, 201903.

van Grunsven, W., Hernandez-Nava, E., Reilly, G.C., Goodall, R., 2014. Fabrication and mechanical characterisation of titanium lattices with graded porosity Metals, 4(3), 401–409.

Hernández-Nava, E., Smith, C. J., Derguti, F., Tammas-Williams, S., Léonar, F., Withers, P. J., Todd, I., Goodall, R. The effect of density and feature size on mechanical properties of isostructural metallic foams produced by additive manufacturing. Acta Materialia, 85 (2015) 387-395.

Lee, H., Zhang, J., Jiang, H., and Fang, N. X., 2012. Prescribed pattern transformation in swelling gel tubes by elastic instability. Phys. Rev. Lett. 108, 214304.

Leonard, A. and Fraternali, F. and Daraio, C., 2013. Directional Wave Propagation in a Highly Nonlinear Square Packing of Spheres. Exp. Mech. 53(3), 327–337.

Liu, Z., Zhang, X., Mao, Y., Zhu, Y. Y., Yang, Z., Chan, C. T., Sheng, P., 2000. Locally resonant sonic materials. Science289, 1734-1736.

Lu, M.H., Feng, L. and Chen, Y. F., 2009. Phononic crystals and acoustic metamaterials. Mater. Today 12, 34–42.

Maldovan, M., 2013. Sound and heat revolution in phononics. Nature 503, 209–217.

Meza, L.R., Das, S. Greer, J., R, 2014. Strong, lightweight, and recoverable three-dimensional ceramic nanolattices. Science 345, 1322–1326.

Milton, G. W. and Cherkaev, A. V., 1995. Which Elasticity Tensors are Realizable? . J. Eng. Mater. Technol. 117(4), 483-493.

Mitchell, S.J., Pandolfi, A., Ortiz, M., 2014. Metaconcrete: designed aggregates to enhance dynamic performance. J. Mech. Phys. Solids 65, 69–81.

Murr, L.E., Gaytan, S.M., Medina, F., Martinez, E., Martinez, J.L., Hernandez, D.H., Machado, B.I., Ramirez, D.a., Wicker, R.B. Characterization of Ti6Al4V open cellular foams fabricated by additive manufacturing using electron beam melting. Materials Science and Engineering: A, 527 (2010) 1861-1868.

Nagase, K. and Skelton, R.E. Minimal Mass Tensegrity Structures. Journal Of The International Association For Shell And Spatial Structures 2014; 55(1):37–48, ISSN:1028-365X.

Nesterenko, V.F. Dynamics of Heterogeneous Materials. Springer-Verlag, New York

Ngo, D. and Fraternali, F. and Daraio, C. (2012). Highly nonlinear solitary wave propagation in Y-shaped granular crystals with variable branch angles. *Phys. Rev. E.*, 85:036602.

Ni, X. Nondestructive Evaluation And Structural Health Monitoring Based On Highly Nonlinear Solitary Waves. Phd Dissertation, University of Pittsburgh, USA.

Oppenheim, I. and Williams, W. Geometric effects in an elastic tensegrity structure. J. Elast. 2000;59:51–65.

Phocas, M.C., Kontovourkis,O., Matheou,M., 2012. Kinetic hybrid structure development and simulation. Int. J. Archit. Comput., 10(1),67–86.

Sakamoto , T., Ferrè, A., Kubo, M. (Eds.), 2008. From Control to Design: Parametric/Algorithmic Architecture. Actar.

Schittny, M., Bckmann, T., Kadic, M., Wegener, M., 2013 Appl. Phys. Lett. , 103, 231905.

Skelton, R. E., de Oliveira, M. C., 2010a. Optimal complexity of deployable compressive structures. J. Franklin I., 347,228–256.

Skelton, R. E., de Oliveira, M. C., 2010b. Optimal tensegrity structures in bending: the discrete Michell truss. J. Franklin I., 347,257–283.

Skelton, R. E., de Oliveira, M. C., 2010c. Tensegrity Systems. Springer.

Skelton, R. E., Nagase, K., 2012. Tensile tensegrity structures. Int. J. Space Struct., 27,131–137.

Skelton, R. E., Fraternali, F., Carpentieri, G., Micheletti, A., 2014. Minimum mass design of tensegrity bridges with parametric architecture and multiscale complexity. Mech. Res. Commun., 58, 124–132.

Smith, C. J., Derguti, F., Hernandez-Nava, E., Tammas-Williams, S., Gulizia, S., Fraser, D., Todd., I. Dimensional accuracy of Electron Beam Melting (EBM) Additive Manufacture with regard to weight optimized truss structures Journal of Materials Processing Technology (Under Review).

Theocharis, G., Boechler, N., Daraio, C, 2013. Nonlinear phononic structures and metamaterials. P.A. Deymier (ed.) Acoustic Matematerials and Phononic Crystals, Springer Series in Solid State Sciences, 173.

Tilbert, A.G., Pellegrino, S., 2011. Review of form-finding methods for tensegritystructures. Space Struct., 18, 209223.

Zheng, X., DeOtte, J., Alonso, M. P., Farquar, G. R., Weisgraber, T. H., Gemberling, S., Lee, H., Fang, N., Spadaccini, C. M. Design and optimization of a light-emitting diode projection micro-stereolithography three-dimensional manufacturing system. Rev. Sci. Instrum., 83 (125001).

Zheng, X., Lee, H., Weisgraber, T. H., Shusteff, M., DeOtte, J., Duoss, E. B., Kuntz, J. D., Biener, M. M., Ge, Q., Jackson, J. A., Kucheyev, S. O., Fang, N. X., Spadaccini, C. M. Ultralight, ultrastiff mechanical metamaterials. Science, 344 (6190):1373–1377.